B: Biophysics; Physical Chemistry of Biological Systems and Biomolecules

One- and Two- Proton Transfer Mechanisms Coexist in One Active Site

Yueqi Zhao, Huaikun Dong, Jing Ren, Jiali Song,
Jianzhuang Yao, Juan Gao, Cheng-Shi Jiang, and Xia Wang

J. Phys. Chem. B, **Just Accepted Manuscript** • DOI: 10.1021/acs.jpcb.0c04445 • Publication Date (Web): 14 Jul 2020

One- and Two-Proton Transfer Mechanisms Coexist in One Active Site

Yueqi Zhao,[a†] Huaikun Dong,[a†] Jing Ren,[a†] Jiali Song,[a] Jianzhuang Yao,[a] Juan Gao,[a]* Cheng-Shi Jiang,[a]* and Xia Wang[a]*

[a]School of Biological Science and Technology, University of Jinan, Jinan 250022, China

[†]These authors contributed equally to this work.

*Correspondence to:

Juan Gao, Ph.D.

Associate Professor, School of Biological Science and Technology

University of Jinan

Jinan 250022, P.R. China

Phone: +86-531-82769122

E-mail: bio_gaoj@ujn.edu.cn

Cheng-Shi Jiang, Ph.D.

Professor, School of Biological Science and Technology

University of Jinan

Jinan 250022, P.R. China

Phone: +86-531-89736799

E-mail: bio_jiangcs@ujn.edu.cn

Xia Wang, Ph.D.

Assistant Professor, School of Biological Science and Technology

University of Jinan

Jinan 250022, P.R. China

Phone: +86-531-82769122

E-mail: bio_wangx@ujn.edu.cn

ABSTRACT

The Acibenzolar S-Methyl (ASM) is one of the most successfully commercialized plants activator of the systemic acquired resistance (SAR). However, its activation (hydrolysis) mechanism catalyzed by the salicylic acid binding protein 2 (SABP2) remains elusive. The fundamental catalytic mechanism of the SABP2-catalzyed hydrolysis of the ASM had been investigated by extensive computational and experimental studies, including QM/MM simulations, charge transfer analysis, small-molecule synthesis, and biochemical assays. Here we report that the promiscuous SABP2 shows different catalytic mechanisms toward different substrates. To catalyze the ASM hydrolysis, the SABP2 uses two-proton transfer mechanism, and the key intermediate is stabilized by the charge transfer effect; to catalyze the ethyl 1,2,3-benzothiadiazole-7-carboxylate (BTM, an ASM analog) hydrolysis, the SABP2 applies the one-proton transfer mechanism, and the classic tetrahedral intermediate is stabilized by the electrostatic effect. The HPLC analyses of the SABP2 esterase activities toward the ASM and the BTM show comparable results with our computaional results, suggesting that the obtained computational mechanism insights are reasonable. The obtained mechanism is not only important supplement to the theory of enzymes' catalytic promiscuity, but also contributes possible strategy for design of next generation plants SAR activators.

Keywords: SABP2; Acibenzolar S-Methyl; SAR; Catalytic Mechanism; Charge Transfer; Oxyanion hole

INTRODUCTION

The systemic acquired resistance (SAR) is widely adopted by plants as an innate defense mechanism against a wide range of phytopathogens.[1] Activation of the SAR in plants requires phytohormones, such as the salicylic acid (SA).[2] In plants, the SA is diffused through cells in its nontoxic methyl form (methyl SA, MeSA).[3] The MeSA is inactive for the SAR activation, but more hydrophobic than the SA. So the MeSA is able to pass through the cell membrances more efficiently than the SA. In the cell of destination, the methyl ester bond of MeSA is hydrolyzed under the help of an esterase named salicylic acid binding protein 2 (SABP2).[4-5] The hydrolysis product (SA) is responsible for the activation of the downstream pathway of the SAR. Exogenous application of the MeSA is able to trigger on the SAR in plants and shows anti-microbial effects.[6] However, accumulation of the SA causes cell toxicity and may lead to cell death in plants.[7] The toxic effect stops the SA from being developped as a plant protection compound.[8]

To overcome the side effects of the SA accumulation, a series of the SA functional analogs (such as benzothiadiazole compounds) had been designed to induce the host defense mechanism (SAR) in plants.[9] Among benzothiadiazoles, the Acibenzolar S-Methyl (ASM) is the first-synthetic in 1987 (EU patent 0313-512; US patent 4-931-581), first-commercialized (BION in Europe and ACTIGARD in the USA), and most-studied plant SAR activator.[8, 10] So far, the ASM has been applied against more than 120 pathosystems (e.g., fungal, bacterial, and virus) in a series of cash crops. For instance, food and cash crops include apple, pear, grapefruit, cucumber, tobacco, cowpea, and so on.[11]

Similarly to the mechanism of the MeSA, the ASM is inactive toward the SAR activation. The ASM hydrolysis catalyzed by the SABP2 is required for the SAR activation,[12] as shown in Figure 1A. The product (1,2,3-Benzothiadiazole-7-carboxylic acid, BCA) is the signal chemical for triggering on the downstream pathway of the SAR. We note that the BCA is not only the hydrolysis product of ASM, but also the hydrolysis product of the methyl

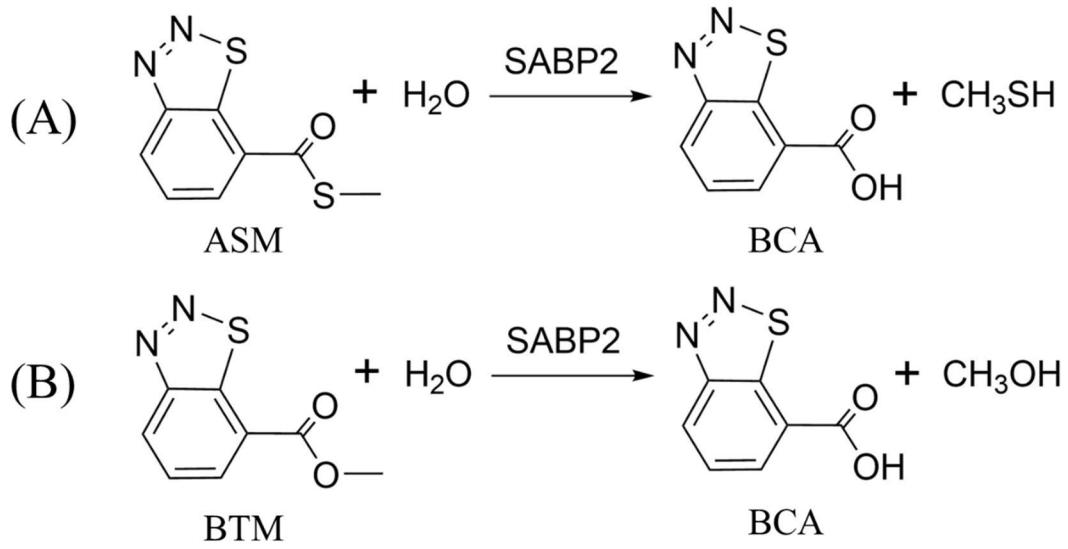

Figure 1. ASM (A) and BTM (B) hydrolysis catalyzed by tobacco SABP2. Acibenzolar-S-Methyl (ASM); 1,2,3-Benzothiadiazole-7-carboxylic acid (BCA); Methyl 1,2,3-benzothiadiazole-7-carboxylate (BTM).

1,2,3-benzothiadiazole-7-carboxylate (BTM). As shown in Figure 1B, whether the SABP2 catalyze the BTM hydrolysis reaction had not been reported. If it is true, questions remain as to whether the BTM is as a good SAR activator as the ASM? Actually, the BTM is first-synthetic in 1970 (British Patent 1176799), and is able to turn on the SAR of plants.[13] Based on comprehensive biological analyses, the ASM stands out as the preferred SAR activator for plants disease control.[8] In other words, the ASM is a better plant-protection chemical than other benzothiadiazoles, including the BTM. The above discussion raises questions as below. First, why is the ASM a better SAR activator than BTM, considering they have the same product (BCA) for the SAR activation? Second, can the BTM be hydrolyzed by the SABP2 to produce the BCA? Third, what are the catalytic mechanisms of the SABP2-catalyzed ASM and BTM hydrolysis? Understanding these questions is helpful for design of next generation plants SAR activators.

In our previous computataional and experimental study,[14] the catalytic mechanism of the SABP2-catalyzed hydrolysis of the MeSA was investigated in detail. The active site of the SABP2 consists of the catalytic triad and the oxyanion hole. The catalytic triad includes Ser81, Asp210, and His238; the oxyanion hole consists of Ala13 and Leu82. The acylation proceeds through two transition states

(TS) and a tetrahedral intermediate (TI). The whole reaction happened in the SABP2-MeSA complex consists of acylation and deacylation processes. The acylation process follows the one-proton transfer mechanism, which is similar with the catalytic mechanism of the serine protease proposed by Arieh Warshel.[15] In the one-proton transfer mechanism, the TSs and TI are stabilized by the electrostatic effect. Particularly, the proton of Ser81 transfers to His238 during the nucleophilic attack. The positively charged His238 sidechain stabilizes the developing negative charge in oxygen atoms of the nucleophile and leaving group. On the other hand, the two-proton transfer mechanism is adopted by many textbooks, and even by the latest textbook of the enzymology.[16] In the two-proton transfer mechanism, two protons transfer concertedly in the catalytic triad. One is from Ser to His, and the other is from His to Asp. The underlying reason of the the two-proton transfer mechanism had not been discussed in detail. Moreover, it seems like that the one- and two-proton transfer mechanisms are contradictory with each other. Therefore, it is of fundamental importance to answer the question whether the one- and two- proton transfer mechanisms can coexist in one active site, as shown in Figure 2. If yes, what are the reasons for the same catalytic triad to adopt different catalytic mechanisms?

To shed light on the abovementioned questions and considerations, extensive computational and experimental studies were performed. First, the fundamental catalytic mechanisms of the ASM and BTM hydrolysis catalyzed by SABP2 were uncovered by the combined quantum mechanics/molecular mechanics (QM/MM), molecular dynamics (MD), and free energy simulations. Then, we synthesized the BTM from the BCA, and the structure of synthetic BTM was confirmed by the ^{1}H, ^{13}C NMR and HRMS spectra. Finally, the relative esterase activities of SABP2 toward BTM and ASM were compared by HPLC chromatogram.

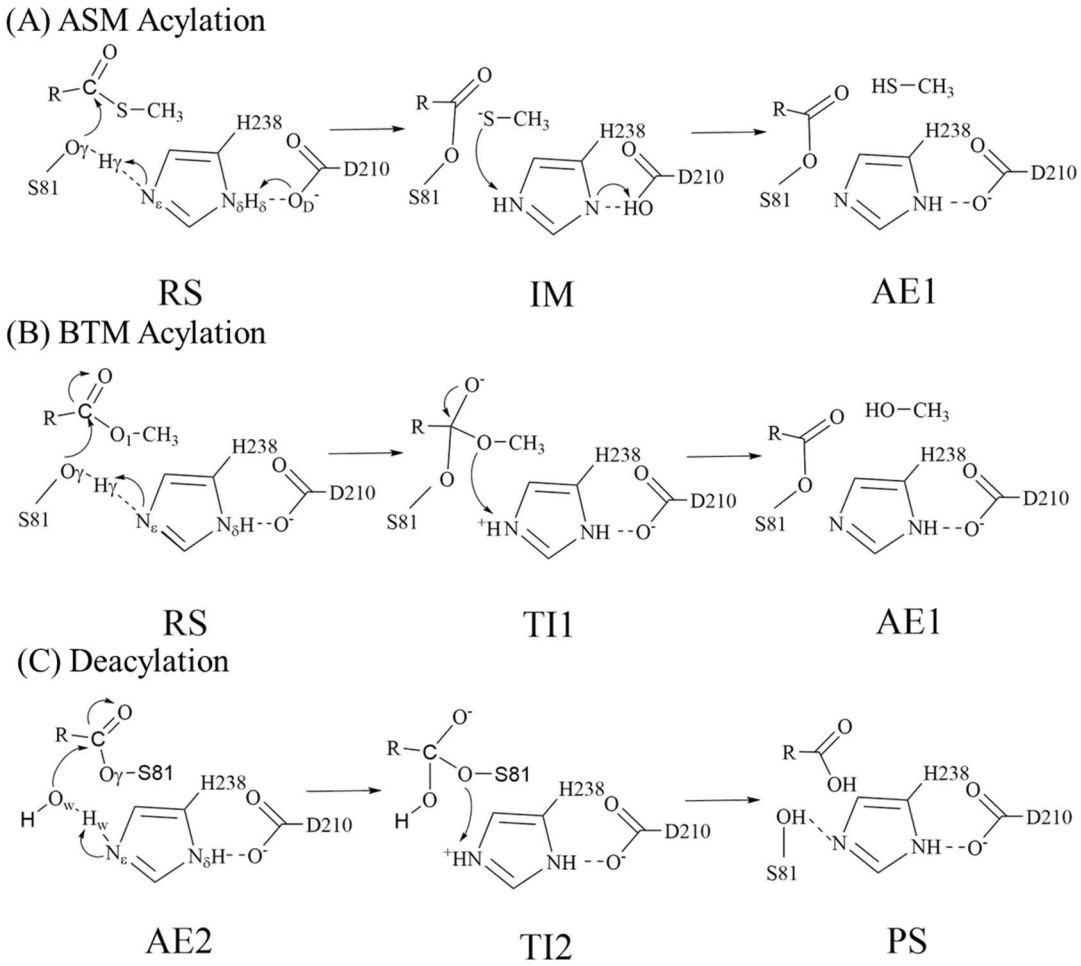

Figure 2. Proposed catalytic reaction mechanisms of SABP2. (A) Acylation process of BTM ester hydrolysis: The one-proton transfer mechanism; (B) Acylation process of ASM thioester hydrolysis: The two-proton transfer mechanism; (C) Deacylation process for both substrates (ASM and BTM): The one-proton transfer mechanism.

METHODS

Computational Details.

Build of two Michaelis-Menten complexes (SABP2-ASM and SABP2-BTM complexes). The initial coordinates and protonation state of SABP2 were obtained from the SABP2-MeSA complex built in our previous study.[14] The ASM and BTM were created by modification of MeSA manually. The Ser81 oxygen (O_γ) atom was chosen as the center of the SABP2 complexes (with ASM and BTM). For the solvation purpose, a 22 Å-radius water droplet was superimposed at the center of the SABP2 complexes. A modified TIP3P water model was applied for description of crystal and solvation water molecules.[17-18] The atoms included in the QM region are the substrates (ASM and BTM) and Ser81, Glu210, and His238 sidechains of the SABP2. All other atoms of the system were included in the MM region. For separation of QM and MM regions, the QM/MM boundaries were divided by link-atoms under the divided frontier charge (DIV) scheme.[19-20] The QM and MM atoms were described by the third-order self-consistent charge density functional tight-binding (DFTB3) method implemented in CHARMM[21-23] and the all-hydrogen CHARMM36m potential function,[24-25] respectively.

QM/MM MD simulation under Stochastic boundary condition[26] with the Ser81 sidechain O_γ atom as the reference center. The reaction region is within 20 Å from the center, and the buffer region includes the atoms from 20 Å to 22 Å. The Newtonian and Langevin equations-of-motion were solved for reaction and buffer regions, respectively. The Langevin thermostat was used and the temperature bath was 300 K. The rest atoms locating outside of reaction and buffer regions were fixed during all simulations. The SHAKE algorithm[27] was applied to constrain the H atom involved covalent bonds. The whole system was first minimized by steepest descent (SD) method and then by adopted-basis Newton-Raphson (ABNR) method. The heating process (from 50K to 298.15K) was performed in 100 ps, and followed by a 1.0 ns production run. The 1-fs time step was used for combined QM/MM MD simulation.

QM/MM Reaction Coordinate Calculations. The reaction-coordinate based adiabatic mapping calculations were started from the last snapshots (close to the average structure) of the production runs at the QM/MM(B3LYP/6-31+G(d,p):CHARMM36m) level by CHARMM interfaced with QChem program,[28] followed by single-point energy calculations at the QM/MM(ωM06-D3/6-311++G(d,p):CHARMM36m) level. All QM/MM reaction-coordinate (adiabatic mapping) calculations were performed to generate the potential energy surfaces along the reaction coordinates (RC) with the force constant of the harmonic constraint (10,000 kcal mol^{-1} $Å^{-2}$). The validation of the reaction-coordinate calculations had been proved by a variety of previous successful calculations on different enzymatic reactions.[29-38]

QM/MM MD and Free energy (potential of mean force, PMF) simulation. After the MD simulations at QM/MM(DFTB3:CHARMM36m) level, the same level PMF free energy simulations were performed using the umbrella sampling method,[39] and the free energy maps as a function of the reaction coordinates (RC) were calculated by the Weighted Histogram Analysis Method (WHAM).[40] For both the acylation and deacylation processes, we first generated the potential energy maps along the RCs by adiabatic mapping calculations at QM/MM(DFTB3:CHARMM36m) level. Totally, more than one hundred windows were simulated in PMF calculations. For a single window, 50 ps MD simulation was performed for equilibration, and 50 ps production run was followed. One snapshot was saved every 0.5 ps. So, a total of 100 snapshots were saved per window. The harmonic biasing potential with a force constant of 150 kcal mol^{-1} $Å^{-2}$ was applied to PMF simulations.

Experimental Details

Synthesis of BTM. The ASM and the BCA were purchased from Dr. Ehrenstorfer GmbH. All of the chemicals used in this study are analytical grade. A mixture of the BCA (50 mg, 0.28 mmol), oxalyl chloride (100 μL) and two drops of *N,N*-dimethylformamide in dry dichloromethane (5 mL) was stirred at room temperature for 1 h. The solvent including the excess oxalyl chloride was removed by

vacuum distillation. The resulting residue was dissolved in dry dichloromethane (2 mL) and then dropped into a mixture of methanol (2 mL) and triethylamine (0.3 mL) with stirring at room temperature. After 12 h of stirring, the mixture was concentrated by vacuum distillation. The obtained residues was purified by flash column chromatography using ethyl acetate/petrol ether (1:4) to give BTM as white solid (28 mg, 52%). ^{1}H NMR (600 MHz, $CDCl_3$): δ 8.84 (d, 1H, J = 8.2 Hz), 8.38 (d, 1H, J = 7.3 Hz), 7.76 (dd, 1H, J = 7.3, 8.2 Hz), 4.07 (s, 3H). ^{13}C NMR (150 MHz, $CDCl_3$): δ 165.4, 158.8, 140.5, 130.6, 128.6, 127.1, 122.9, 53.2. HRESIMS: m/z calcd for $C_8H_7N_2O_2S^+$ 195.0223, found 195.0220.

Expression and Purification of SABP2. The protocal of SABP2 expression and purification is described in a previous study with minor modifications.[4] Briefly, the tobacco SABP2 (GenBank ID: AY485932) with a 6xHis-tag at C-terminal was cloned into the plasmid pET21 (Novagen). The generated plamid pET21-SABP2 was verified by the DNA sequence analysis with T7 promoter and terminator, and then transformed into *E. coli* strain BL21 (DE3) cells (Invitrogen, Carlsbad, CA). The recombinant SABP2 was purified from *E. coli* cell lysate using Ni-NTA agarose, followed by dialysis. The purity of the SABP2 was verified by SDS-PAGE.[41] The concentration (more than 1.0 μg/μl) of purifed SABP2 was determined by the Bradford assay.

SABP2 Esterase Assays. The method of SABP2 esterase assays was described in a previous study with minor modification.[12] The HPLC was applied to monitor the esterease reactions catalyzed by SABP2 toward the substrates including the ASM and BTM. The C18 reverse-phase analytical column was applied for the HPLC analysis. The mobile phase of HPLC is 80% methanol (HPLC grade) with 0.3% trifluoroethanoic acid (TFA). The flow rate is 0.7 ml/min. The absorbance of the substrates (ASM and BTM) and product (BCA) was monitored at 255 nm. The reaction assays of SABP2 toward ASM and BTM were carried out at 30℃ in 0.1M phosphate buffer (pH 7.2) with 10% acetonitrile for the sake of low solubility of the

substrates. The reaction time is 10 minutes before the injection of reaction mixture into the HPLC.

Table 1. Key Distances for Reactions Occurred in the SABP2.

Substrates	State	Bond Length (Å)								
		d(O_γ…C)	d(O_γ…H_γ)	d(S…C)	d(Nε…H_γ)	d(N_δ…H_δ)	d(O_D…H_δ)	d(A13…O)	d(L82…O)	d(S…H_γ)
ASM-Acylation	RS-average	2.92±0.11	0.98±0.03	1.72±0.04	2.10±0.19	1.03±0.03	1.80±0.15	2.41±0.32	3.09±0.22	
	RS	2.73	1.02	1.79	1.64	1.07	1.51	1.95	2.81	
	TS1	2.04	1.48	1.85	1.10	1.12	1.40	1.90	2.25	
	IM	1.34	2.71	3.43	1.04	1.58	1.04	1.98	1.86	2.31
	TS2	1.33	2.95	3.59	1.62	1.14	1.39	1.95	1.88	1.47
	AE1	1.33	3.28	3.69	2.74	1.04	1.65	1.96	1.90	1.35
BTM-Acylation		d(O_γ…C)	d(O_γ…H_γ)	d(O_1…C)	d(Nε…H_γ)	d(N_δ…H_δ)	d(O_D…H_δ)	d(A13…O)	d(L82…O)	d(O_1…H_γ)
	RS-average	3.05±0.15	0.99±0.03	1.35±0.03	1.93±0.17	1.04±0.03	1.80±0.15	2.03±0.20	3.21±0.26	
	RS	2.65	1.02	1.34	1.62	1.06	1.59	1.88	2.61	3.32
	TS1	1.90	1.50	1.40	1.09	1.10	1.46	1.88	2.13	3.03
	TI1	1.49	1.75	1.49	1.04	1.15	1.37	1.89	1.90	2.88
	TS2	1.41	2.45	1.71	1.05	1.11	1.48	2.02	1.99	1.75
	AE1	1.35	2.66	2.55	1.86	1.06	1.68	2.00	1.87	0.99
Deacylation		d(O_γ…C)	d(O_γ…H_w)	d(O_w…C)	d(O_w…H_w)	d(Nε…H_w)	d(N_δ…H_δ)	d(O_D…H_δ)	d(A13…O)	d(L82…O)
	AE2	1.34	2.63	3.04	0.99	1.87	1.04	1.79	1.95	1.89
	TS3	1.43	2.43	1.83	1.07	1.51	1.05	1.73	1.95	2.07
	TI2	1.55	1.72	1.45	3.05	1.05	1.10	1.47	1.81	1.86
	TS4	1.89	1.51	1.39	3.14	1.10	1.08	1.52	1.81	1.95
	PS	2.65	1.01	1.35	3.47	1.66	1.05	1.63	1.81	2.30

See Figure 2 for atom labels.

RESULTS AND DISCUSSION

It has been reported that the SABP2 belongs to the α/β fold superfamily of hydrolases.[4] The reaction mechanism of SABP2-catalyzed hydrolysis of MeSA had been investigated in detail by our previous compuational and experimental study.[14] In this study, we further investigated the reaction mechanism of SABP2 catalyzed hydrolysis of ASM and BTM to shed light on how different reaction mechanisms happen in one active site. Key distances for all reaction states are listed in Table 1.

Michalis−Menten complexes of SAPB2 with ASM or BTM. Average structures of the reactant states of SABP2 with the ASM (depicted in Figure S1A) and the BTM (depicted in Figure S1B) were obtained by QM/MM(DFTB3/CHARMM36m) MD simulations. By comparison of the SABP2 reactant states of the ASM and the BTM, both average structures share similar properties with each other. For example, stable hydrogen bond networks are observed in both catalytic triads (consisting of Ser81, Asp210, and His238) of the ASM and the BTM complexes. Both substrates form one hydrogen bond with backbone amide group of Ala13 in the oxyanion hole of SABP2. The distance between the nucleophilic oxygen of Ser81 side chain and the methyl ester group carbonyl carbon of the BTM is 3.05±0.15 Å, and the distance between the nucleophilic oxygen of Ser81 side chain and the methyl thioester group carbonyl carbon of the BTM is 2.92±0.11 Å. Two distances for the nucleophilic attacks are close to each other (no significant difference). The only significant difference between two reactants is the substrates. The ASM contains a methyl thioester, while the BTM contains a methyl ester. However, neither of them gets involved in the direct interaction with the active site of SABP2. In the reactant states, the ASM and the BTM share similar binding properties with the active site of the SABP2.

Acylation Reaction Pathway Involving ASM. The reaction coordinate calculation was carried out at the QM/MM(B3LYP/6-31+G(d,p):CHARMM36m) level, followed by the single point energy calculation at the QM/MM(ωM06-D3/6-311++G(d,p):CHARMM36m) level. The obtained potential energy profile shows that the acylation of the SABP2-ASM reaction pathway is a

two-step process with two TSs and an IM, as shown in Figures 2A and S2A. The first step of the acylation happens along with the nucleophilic attack by Ser81 sidechain, and the reaction coordinate calculation of first step was simulated with RC1. During the first step in Figures S2B-D, a new covalent bond (C-Oγ) forms and a covalent bond (C-S) breaks, simutaneously. Notably, two protons (e.g., Hγ and H_δ) tranfer at the same time. The Hγ is transferred from the Oγ of Ser82 to the Nε of His238, while the H_δ is transferred from the His238 N_δ atom to the O_D of Asp210. During the reaction process from the RS to the IM, the distance decreases between the carbonyl oxygen of the ASM and the Leu82 amide group of the oxyanion hole, indicating a gradual enhancement of oxyanion hole stabilization for the developping negative charge of the ASM carbonyl oxygen. At the end of the first step (IM), the thioester bond (C-S) is completely broken with an optimized distance of 3.43 Å. Starting from IM, the second step was simulated with RC2, and ends in AE1 state by crossing the TS2. As shown in Figures S2D-F, the bond forming and breaking involved in the second step can mainly be reflected by two concerted proton transfer processes. One is that the Hγ leaves the His238 side chain, moves to the S atom of the ASM, and forms a methanthiol (the product of the acylation). The other is that the H_δ is transferred back from the Asp210 sidechain to the His238 sidechain. The hydrogen bonds of the oxyanion hole (forming by Ala13 and Leu82) keep almost the same during the the two-proton transfer process from IM to AE1. Overall, the QM/MM reaction coordinate calculation demonstrates that the acylation process of SABP2-ASM complex adopts a the two-proton transfer mechanism rather than the one-proton transfer mechanism adopted by the SAPB2 catalyzed hydrolysis of its native substrate (MeSA). Thus, it is interesting to understand the origin of the SABP2 catalytic promiscuity.

Acylation Reaction Pathway Involving BTM. To eluciate the SABP2 catalytic promisuity toward the ester bond and the thioester bond, we studied the reaction mechanism of the SABP2 catalyzed hydrolysis of the BTM. The ASM contains a thioester bond, while the BTM contains an ester bond to be hydrolyzed by SABP2.

The reaction coordinate (RC3) and single point energy calculations for the SABP2-BTM complex were performed at the same QM/MM levels with SABP2-ASM complex. The obtained potential energy profile shows that the acylation of SABP2-BTM reaction pathway is a two-step process with two TS and a TI1 states, as shown in Figures 2B and S3A. Overall, the acylation process of the SABP2-BTM reaction follows a classic serine esterase reaction pathway, in which the nucleophilic attack by Ser82 side chain results in forming of the new covalent bond (C-Oγ) in the first step and breaking of the existing covalent bond (C-O_1) in the second step. As shown in Figures S3B-D, the first step is from RS to TI1. In TI1, the new covalent bond (C-Oγ) has formed, but the covalent bond (C-O_1) has not yet broken. The TI1 is a classic tetrahedral intermediate stabilized by the positively charged His238 side chain and the enhanced oxyanion hole. Only one proton (Hγ) is transferred to His238 side chain, and the positive charge on His238 is electrostatically stabilized by the negative charge on the Asp210 sidechain. The second step of the acylation starts from the TI1 and ends in the AE1, as shown in Figures S3D-F. In the TS2, the covalent bond (C-O_1) has partly broken; the proton (Hγ) is leaving the His238 sidechain and transferring to the O_1 atom. At the AE1, the product of acylation (methanol) is formed. Overall, acylations of the SABP2 catalyzed hydrolysis of ASM and BTM are different with each other in two ways. One is the intermediates are different. The other is the ASM adopts thetwo-proton transfer mechanism, while the BTM adopts the one-proton transfer mechanism. The results show that the catalytic mechanism of the SABP2 not only depends on enzyme itself, but also depends on substrates.

Deacylation Reaction Pathway. After the acylation processes of the ASM and the BTM in SABP2, the acylation products (methanthiol for ASM and methanol for BTM) leave the active site. Instead, water molecules get into the active site to form the AE2 state. From the beginning of deacylation (AE2), the ASM and the BTM with the SABP2 share the same deacylation mechanism catalzyed, as shown in Figures 2C and S4. Reaction coordinate (RC4) and single point energy calculations for the deacylation were performed at the same QM/MM levels with two acylation processes.

As shown in Figures S4B-F, the deacylation process follows the classic serine esterase mechanism: 1) it starts from the AE2, crosses two TSs and one TI2, and finally ends in PS; 2) the negative charge on TI2 is stabilized by both oxyanion hole and positive charge on His238 side chain from the one-proton transfer mechanism; 3) forming and breaking covalent bonds along with the nucleophilic attack are (C-O_w) and (C-Oγ), respectively.

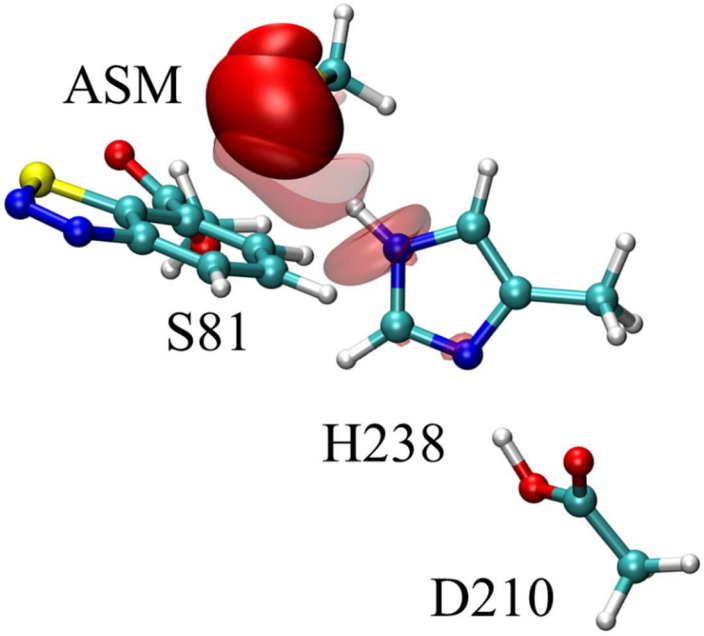

Figure 3. Two most significant COVPs in the IM complex calculated at the QM/MM(wM06-D3/6-311++G(d,p):CHARMM36m) level. The isosurface value is 0.05. Occupied orbitals are presented by solid color, while complementary virtual orbitals are presented by transparent color. Only QM atoms including link atoms are shown for clarity.

Charge Transfer Effects in Two-proton transfer Mechanism. It is interesting to understand the origin of the one- and two- proton transfer mechanisms happening in one active site. The difference between the one- and two- proton transfer mechanisms is whether the H_δ atom of the His238 is transferred to Asp210 side chain during the reaction, as shown in Figure 2. In the one-proton transfer mechanism, the Hγ atom of the Ser81 is transferred to the His238 side chain, but the H_δ atom stays in the side chain of the His238. As a result, the protonated His238 side chain is positively charged. The positive charge of the His238 hydrogen atoms (Hγ and H_δ) helps to stabilize the negative charge of oxygen atoms of both nucleophile and leaving group. The negative charge of the Asp210 side chain helps to stabilize the positive

charge on the His238 by electrostatical effect. Indeed, the calculated mulliken charges of Hγ atom in TI1 and TI2 are around 0.4 at the QM/MM(ωM06-D3/6-311++G(d,p):CHARMM36m) level by Q-chem/CHARMM program. In the two-proton transfer mechanism, the Hγ and H_δ hydrogen atoms are transferred to the side chains of the His238 and the Asp210, respectively. As a result, the His238 and Asp210 side chains are neutral in the IM (Figure S2D). Surprisingly, the calculated mulliken charges of the Hγ atom in the IM is -0.1. The Hγ atom shows uncommon negative partial charge, which is significantly different with the Hγ atom of TI states (positive partial charge). These interesting findings encourage us to propose that a charge transfer happens between the deprotonated methanthiol and the side chain of the His238.

The intermolecular interactions can be analyzed by the absolutely localized molecular orbitals (ALMOs) based energy decomposition analysis (EDA) and the charge transfer analysis (CTA) implemented in Q-Chem.[42] The ALMOs based EDA and CTA had been successfully applied to analyze the energy lowering induced by the charge transfer in many cases, such as hydrogen bond in water dimer.[43] In this study, we investigated the charge donor and acceptor interactions (especially hydrogen bonding interaction) between the deprotonated methanthiol and the rest of the enzyme-substrate complex (especially the side chain of the His238) in the IM state of the SABP2-ASM acylation process by the ALMOs based EDA and CTA at the QM/MM(ωM06-D3/6-311++G(d,p):CHARMM36m) level. The EDA and CTA methods divide the total interaction energy into charge transfer energies (CT), a polarization energy (POL), and a frozen density interaction energy (FRZ) in Table 2. All of them (CT, POL, and FRZ) contribute the favorable energy to the stabilization of IM state. In the IM complex, the forward charge transfer (ΔQ) from the deprotonated methanthiol to the rest of the system is 17.0 mē, and the backward charge transfer from the rest of the system to the deprotonated methanthiol is 0.2 mē. The corresponding energy change (ΔE) are -6.7 kcal/mol and -0.1 kcal/mol, respectively. The ΔQ of the higher order charge transfer (HO-CT) is 13.0 mē that

contributes -2.1 kcal/mol energy lowering. The counterpoise corrections to the charge transfer (e.g., BSSE and RS-BSSE) are very small. The forward and backward charge transfer and associated energy terms can be further described in terms of molecular orbital contributions by the complementary occupied-virtual orbital pairs (COVPs) analysis.[42] In each COVP, the charge transfer is from an occupied orbital on one molecule to a complementary virtual orbital on the other molecule. The COVPs decomposition shows that 88.2% of ΔQ (D→A: from the deprotonated methanthiol to the rest of the system) and 89.6% of ΔE (D→A) are from two most significant COVPs. In Figure 3, the two most important COVPs in IM complex mainly result from the charge transfer (electron donation) from the negative charged sulphur's sp^3-hybridized lone pairs (occupied orbital) in the deprotonated methanthiol to the virtual orbital (resembling the N–H σ-antibonding orbital) in the His238 side chain. Based on these results, we conlcude that the two-proton transfer transfer mechanism happened in IM state can be partly stabilized by the charge transfer induced energy lowering effect (about 8.9 kcal/mol).

Table 2. ALMO CTA and EDA results for the IM. Complex is optimized at the QM/MM(B3LYP/6-31+G(d,p)) level, decomposition analysis is performed at the QM/MM(ωM06-D3/6-311++G(d,p)) level. All terms are corrected for BSSE.

Scale	ΔQ [mē]	ΔE [kcal/mol]
FRZ	0.0	-19.2
POL	0.0	-12.6
CT(D→A)[a]	17.0	-6.7
CT(A→D)	0.2	-0.1
HO-CT	13.0	-2.1
Total	28.8	-40.7
BSSE	2.2	0.9
RS-BSSE	1.3	0.7
$COVP_2$[b]	88.2%	89.6%

[a] A= electron acceptor, D=electron donor; [b] Contribution of two most significant COVPs is given as percentage of CT(D→A).

The one- and two- proton transfer reactions occurred in the SABP2 might be correlated to different leaving groups of the substrates (BTM and ASM). Along with the nucleophilic attack by the Ser81, different substrates generate different leaving groups. For the ASM, the leaving group is the deprotonated methanthiol (CH_3S^-,

depicted in Figure 2A); for the BTM, the leaving group is the deprotonated methanol (CH_3O^-, depicted in Figure 2B).

Regarding to the active site of the SABP2, key difference of the one- and two-proton transfer mechanisms is different protonation states of the His238 sidechain. In the one-proton transfer mechanism, the protonated His238 sidechain is positively charged in TI1 state; in the two-proton transfer mechanism, the His238 sidechain is neutrally charged. It has been widely discussed that the positively charged Histidine sidechain of the classic catalytic triad is necessary for stabilization of the developing negative charge of TSs and TIs along with the nucleophilic attack.[15] So, the question is why the deprotonated methanthiol in the SABP2-BTM IM state does not need the electrostatic stabilization from the positive charged His238.

Reactions with better leaving groups happen in a faster rate compared to reactions with worse leaving groups.[44] In comparison of the acylation processes, we found the ASM shows a much lower transition state barrier than the BTM. The result implies that the CH_3S^- is a better leaving group compared to the CH_3O^-. Indeed, the pKa of the CH_3S^- conjugate acid (CH_3SH) is 10.4, while the pKa of the CH_3O^- conjugate acid (CH_3OH) is 15.5. Because the CH_3S^- is a better leaving group than the CH_3O^-, the CH_3S^- owns a better ability to stabilize its negative charge, and forms a more stable anion. Additionally, the CH_3S^- transfers its partial negative charge to the sidechain of His238. Therefore, the CH_3S^- as a stable anion does not require extra electrostatic effect from the positive charged His238 to stabilize its negative charge. Under this circumstance, the His238 transfers its H_δ atom to the Asp210 O_D atom; the neutrally charged His238 and Asp210 are formed in the IM state.

Overall, the one- and two- proton transfer mechanisms occurring in one active site of the SABP2 may due to the following two reasons. One is that the ASM CH_3S^- is a better leaving group than the BTM CH_3O^-. The other is the charge transfer occurs in the ASM CH_3S^-. These two reasons make the ASM leaving group (CH_3S^-) a more stable anion, so the positive charged His238 sidechain (in other words, the two-proton transfer mechanism) is not necessary. The underlying reason for the charge transfer needs to be investigated further. For instance, similar computational and experimental strategy might be applied to the SABP2-catalzyed esterase reactions to different

substrates with the same leaving group (the deprotonated methanthiol).

Comparison with Experimental Data. The calculated potential energy barriers for the SABP2-ASM (Figure S2A), the SABP2-BTM (Figure S3A) acylations, and the deacylation (Figure S4A) are 9.5 kcal/mol, 18.7 kcal/mol, and 18.6 kcal/mol, respectively. Then, QM/MM(DFTB3/CHARMM36m) PMF simulations were carried out to calcuate the entropy contributions to the rate-limiting steps of the ASM and the BTM hydrolyses catalyzed by the SABP2. Since it is too computationally expensive to perform PMF calculations by the high-level DFT methos, the entropy contributions were estimated by the DFTB3 based methods[38, 45-46] As shown in Figures S5 and S6, the energies of entropy contributions to the rate-limiting TSs of the SABP2-BTM acylation and deacylation are -1.5 kcal/mol and -0.5 kcal/mol, respectively. In other words, the deacylation is the rate-limiting process for the SABP2 catalyzed hydrolyses of the ASM and the BTM, and thus the activation free energy barriers of the SABP2-ASM and the SABP2-BTM are identical to each other.

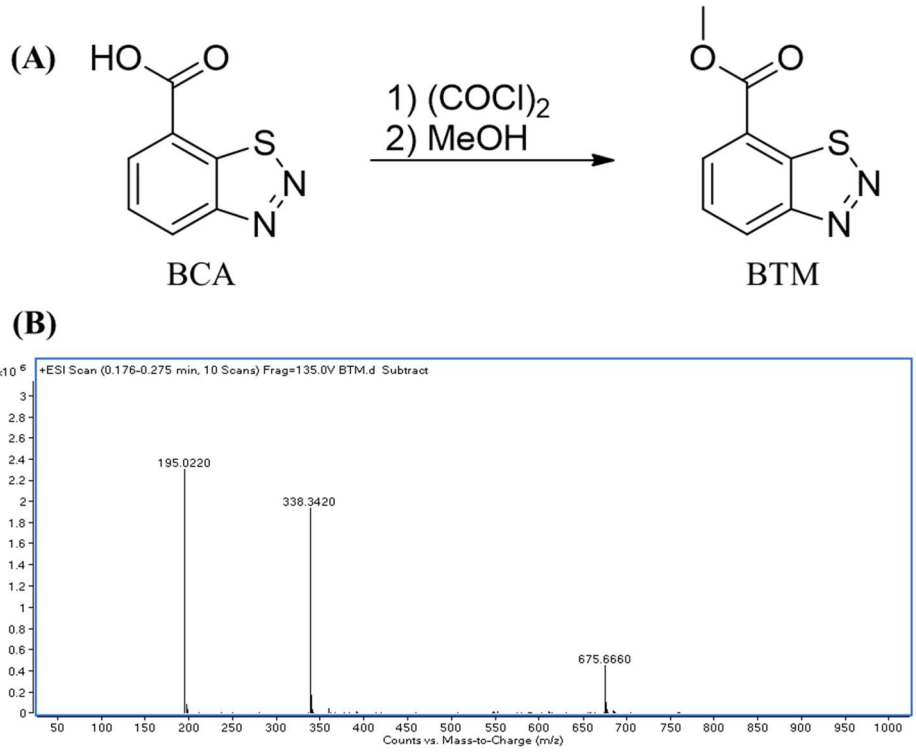

Figure 4. The synthesis of BTM. (A) Reaction conditions: 1) oxalyl chloride, N,N-dimethylformamide, dichloromethane, r.t., 1 h; 2) methanol, triethylamine, dichloromethane, r.t., overnight, yield 52%. (B) HRESIMS spectrum of BTM.

In order to prove the theoretical prediction that the SABP2-ASM and the SABP2-BTM hydrolyses share the same activation free energy barrier, the *in vitro* enzymatic experiments were carried out to compare the esterase activities between the SABP2 catalyzed hydrolyses of the ASM and the BTM. As shown in Figures 4, S7, and S8, the substrate (BTM) was synthesized from BCA by an established method,[47] and was further proved by HRESIMS spectra and NMR. In Figure 5A, the HPLC result shows that the ASM runs faster than the BTM, indicating the ASM is more hydrophobic than the BTM. The hydrophobic nature of the ASM may partly account for its better performance as a pestcide compared to the BTM. It has been reported that the ASM performs 15 folds better than the SA (K_d = 90 nM) for binding with the SABP2.[48] The MeSA is suggested to share a similar binding affinity to the SABP2 with the SA, and the K_m for the SABP2-MeSA esterase reaction is 8.6 μM.[4] Thus, it is reasonable to speculate that the K_m for the SABP2-ASM esterase reaction may be at least 10 folds smaller than the K_m for the SABP2-MeSA esterase reaction. Also, the BTM who shares a similar molecular structure with the ASM is expected to share a similar K_m with the ASM for binding to the SABP2. Indeed, our HPLC analyses show that both K_m values of the SABP2 catalyzed hydrolyses of the ASM and the BTM are much smaller than the limitation of detect (around 2 μM) of HPLC analysis. To compare the SABP2's esterase actitivies toward the ASM and the BTM, the enzyme assays were performed under three substrates concentrations (e.g., 40 μM, 45μM, and 50 μM). As shown in Figure 5B, the reaction rates of the SABP2 toward the ASM and BTM are similar to each other at three substrate concentrations. Overall, the experimental results agree well with the theoretical prediction, indicating our computational mechanism insights are reasonable.

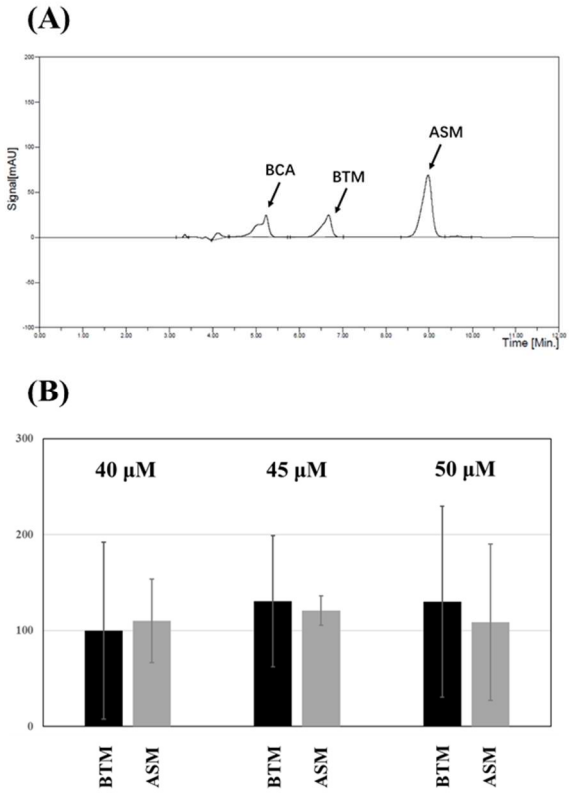

Figure 5. Experimental study of SABP2 catalyzed hydrolyses of ASM and BTM. (A) HPLC chromatogram of 50µM pure ASM, BTM, and BCA in acetonitrile, respectively. HPLC analysis was used to monitor the enzymatic activity of SABP2. A C-18 column connected to a HPLC with UV detector was used for the analysis. Samples were injected in total volume of 20 µl and monitored at 255 nm. (B) Relative methyl esterase activity of SABP2 with BTM and ASM at three different concentrations (40 µM, 45 µM, and 50 µM). The activity with BTH at 40µM was set at 100%.

CONCLUSION

Many enzymes have been reported because of their remarkable properties of the catalytic promiscuity.[49] However, our understanding of the catalytic promiscuity of enzymes is still lacking. In this study, the catalytic promiscuity of the SABP2 toward the ASM (a thioester) and BTM (an ester) were investigated both computationally and experimentally. Interestingly, our results show that the SABP2 catalzyed ASM thioester hydrolysis adopts the two-proton transfer mechanism, while the SABP2 catalzyed BTM thioester hydrolysis adopts the one-proton transfer mechanism. In the single active site of the SABP2, the two-proton transfer mechanism is stabilized by charge transfer effect in IM state, while the one-proton transfer mechanism is stabilized by electrostatic effect. Our results therefore support the hypothesis of the mechanism promiscuity that the promiscuous enzymes adopt different catalytic mechanisms toward different kinds of reactions (substrates). For further design of plants SAR activators based on the ASM, one design strategy may be lowering the activation free energy barrier of the SABP2-ASM deacylation process. As a result, the accumulation of the BCA may be accelerated, and the effectiveness of the ASM as a pestcide might be significantly improved.

Supporting Information

Figures for additional computational and experimental data and results.

Corresponding Author

E-mail: bio_gaoj@ujn.edu.cn

E-mail: bio_jiangcs@ujn.edu.cn

E-mail: bio_wangx@ujn.edu.cn

ORCID

Jianzhuang Yao: 0000-0002-5017-3677

Notes

The authors declare no competing interest.

ACKNOWLEDGEMENTS

We thank fundings from the National Natural Science Foundation of China (grant 21703079), the Shandong Provincial Natural Science Foundation, China (grants ZR2017BB056) for supporting this work.

Reference

(1) Ryals, J. A.; Neuenschwander, U. H.; Willits, M. G.; Molina, A.; Steiner, H. Y.; Hunt, M. D., Systemic Acquired Resistance. *The Plant Cell* **1996,** *8*, 1809-1819.

(2) Park, S.-W.; Kaimoyo, E.; Kumar, D.; Mosher, S.; Klessig, D. F., Methyl Salicylate Is a Critical Mobile Signal for Plant Systemic Acquired Resistance. *Science* **2007,** *318*, 113-116.

(3) Kumar, D., Salicylic Acid Signaling in Disease Resistance. *Plant Sci.* **2014,** *228*, 127-134.

(4) Forouhar, F.; Yang, Y.; Kumar, D.; Chen, Y.; Fridman, E.; Park, S. W.; Chiang, Y.; Acton, T. B.; Montelione, G. T.; Pichersky, E., et al., Structural and Biochemical Studies Identify Tobacco Sabp2 as a Methyl Salicylate Esterase and Implicate It in Plant Innate Immunity. *Proc. Natl. Acad. Sci. U.S.A.* **2005,** *102*, 1773-1778.

(5) Kumar, D.; Klessig, D. F., High-Affinity Salicylic Acid-Binding Protein 2 Is Required for Plant Innate Immunity and Has Salicylic Acid-Stimulated Lipase Activity. *Proc. Natl. Acad. Sci. U.S.A.* **2003,** *100*, 16101-16106.

(6) Silverman, F. P.; Petracek, P. D.; Heiman, D. F.; Ju, Z.; Fledderman, C. M.; Warrior, P., Salicylate Activity. 2. Potentiation of Atrazine. *J. Agric. Food. Chem.* **2005,** *53*, 9769-9774.

(7) Cronjé, M. J.; Weir, I. E.; Bornman, L., Salicylic Acid-Mediated Potentiation of Hsp70 Induction Correlates with Reduced Apoptosis in Tobacco Protoplasts. *Cytometry Part A* **2004,** *61A*, 76-87.

(8) Friedrich, L.; Lawton, K.; Ruess, W.; Masner, P.; Specker, N.; Rella, M. G.; Meier, B.; Dincher, S.; Staub, T.; Uknes, S., et al., A Benzothiadiazole Derivative Induces Systemic Acquired Resistance in Tobacco. *The Plant Journal* **1996,** *10*, 61-70.

(9) Toquin, V.; Sirven, C.; Assmann, L.; Sawada, H., Host Defense Inducers. In *Modern Crop*

Protection Compounds, Wiley-VCH Verlag GmbH & Co. KGaA: Weinheim, Germany, 2012; pp 909-928.
(10) Tripathi, D.; Pappu, H. R., Evaluation of Acibenzolar-S-Methyl-Induced Resistance against Iris Yellow Spot Tospovirus. *Eur. J. Plant Pathol.* **2015,** *142*, 855-864.
(11) Tripathi, D.; Raikhy, G.; Kumar, D., Chemical Elicitors of Systemic Acquired Resistance—Salicylic Acid and Its Functional Analogs. *Current Plant Biology* **2019,** *17*, 48-59.
(12) Tripathi, D.; Jiang, Y.-L.; Kumar, D., Sabp2, a Methyl Salicylate Esterase Is Required for the Systemic Acquired Resistance Induced by Acibenzolar-S-Methyl in Plants. *FEBS Lett.* **2010,** *584*, 3458-3463.
(13) Kunz, W.; Schurter, R.; Maetzke, T., The Chemistry of Benzothiadiazole Plant Activators. *Pestic. Sci.* **1997,** *50*, 275-282.
(14) Yao, J.; Guo, H.; Chaiprasongsuk, M.; Zhao, N.; Chen, F.; Yang, X.; Guo, H., Substrate-Assisted Catalysis in the Reaction Catalyzed by Salicylic Acid Binding Protein 2 (Sabp2), a Potential Mechanism of Substrate Discrimination for Some Promiscuous Enzymes. *Biochemistry* **2015,** *54*, 5366-5375.
(15) Warshel, A.; Naray-Szabo, G.; Sussman, F.; Hwang, J. K., How Do Serine Proteases Really Work? *Biochemistry* **1989,** *28*, 3629-3637.
(16) Purich, D. L., In *Enzyme Kinetics: Catalysis & Control*, Purich, D. L., Ed. Elsevier: Boston, 2010.
(17) Jorgensen, W. L., Quantum and Statistical Mechanical Studies of Liquids .10. Transferable Intermolecular Potential Functions for Water, Alcohols, and Ethers - Application to Liquid Water. *J. Am. Chem. Soc.* **1981,** *103*, 335-340.
(18) Neria, E.; Fischer, S.; Karplus, M., Simulation of Activation Free Energies in Molecular Systems. *J. Chem. Phys.* **1996,** *105*, 1902-1921.
(19) Field, M. J.; Bash, P. A.; Karplus, M., A Combined Quantum-Mechanical and Molecular Mechanical Potential for Molecular-Dynamics Simulations. *J. Comput. Chem.* **1990,** *11*, 700-733.
(20) Brooks, B. R.; Brooks, C. L.; Mackerell, A. D.; Nilsson, L.; Petrella, R. J.; Roux, B.; Won, Y.; Archontis, G.; Bartels, C.; Boresch, S., et al., Charmm: The Biomolecular Simulation Program. *J. Comput. Chem.* **2009,** *30*, 1545-1614.
(21) Cui, Q.; Elstner, M.; Kaxiras, E.; Frauenheim, T.; Karplus, M., A Qm/Mm Implementation of the Self-Consistent Charge Density Functional Tight Binding (Scc-Dftb) Method. *J. Phys. Chem. B* **2001,** *105*, 569-585.
(22) Gaus, M.; Cui, Q.; Elstner, M., Dftb3: Extension of the Self-Consistent-Charge Density-Functional Tight-Binding Method (Scc-Dftb). *J. Chem. Theory Comput.* **2011,** *7*, 931-948.
(23) Yang; Yu, H.; York, D.; Cui, Q.; Elstner, M., Extension of the Self-Consistent-Charge Density-Functional Tight-Binding Method: Third-Order Expansion of the Density Functional Theory Total Energy and Introduction of a Modified Effective Coulomb Interaction. *J. Phys. Chem. A* **2007,** *111*, 10861-10873.
(24) MacKerell, A. D.; Bashford, D.; Bellott, M.; Dunbrack, R. L.; Evanseck, J. D.; Field, M. J.; Fischer, S.; Gao, J.; Guo, H.; Ha, S., et al., All-Atom Empirical Potential for Molecular Modeling and Dynamics Studies of Proteins. *J. Phys. Chem. B* **1998,** *102*, 3586-3616.
(25) Huang, J.; Rauscher, S.; Nawrocki, G.; Ran, T.; Feig, M.; de Groot, B. L.; Grubmüller, H.; MacKerell Jr, A. D., Charmm36m: An Improved Force Field for Folded and Intrinsically Disordered Proteins. *Nat. Methods* **2017,** *14*, 71-73.

(26) Brooks, C. L.; Brunger, A.; Karplus, M., Active-Site Dynamics in Protein Molecules - a Stochastic Boundary Molecular-Dynamics Approach. *Biopolymers* **1985,** *24*, 843-865.
(27) Ryckaert, J. P.; Ciccotti, G.; Berendsen, H. J. C., Numerical-Integration of Cartesian Equations of Motion of a System with Constraints - Molecular-Dynamics of N-Alkanes. *J. Comput. Phys.* **1977,** *23*, 327-341.
(28) Shao, Y.; Gan, Z.; Epifanovsky, E.; Gilbert, A. T. B.; Wormit, M.; Kussmann, J.; Lange, A. W.; Behn, A.; Deng, J.; Feng, X., et al., Advances in Molecular Quantum Chemistry Contained in the Q-Chem 4 Program Package. *Mol. Phys.* **2015,** *113*, 184-215.
(29) Yao, J.; Yuan, Y.; Zheng, F.; Zhan, C.-G., Unexpected Reaction Pathway for Butyrylcholinesterase-Catalyzed Inactivation of "Hunger Hormone" Ghrelin. *Sci. Rep.* **2016,** *6*, 22322.
(30) Wang, X.; Yao, J., Improvement of the Self-Consistent-Charge Density-Functional-Tight-Binding Theory by a Modified Mulliken Charge. *Theor. Chem. Acc.* **2017,** *136*, 124.
(31) Yao, J.; Luo, H.; Wang, X., Understanding the Catalytic Mechanism and the Substrate Specificity of an Engineered Gluten Hydrolase by Qm/Mm Molecular Dynamics and Free Energy Simulations. *J. Chem. Inf. Model.* **2017,** *57*, 1179-1186.
(32) Yao, J.; Wang, X.; Luo, H.; Gu, P., Understanding the Catalytic Mechanism and the Nature of the Transition State of an Attractive Drug-Target Enzyme (Shikimate Kinase) by Quantum Mechanical/Molecular Mechanical (Qm/Mm) Studies. *Chem. - Eur. J.* **2017,** *23*, 16380–16387.
(33) Wang, X.; Li, R.; Cui, W.; Li, Q.; Yao, J., Qm/Mm Free Energy Simulations of an Efficient Gluten Hydrolase (Kuma030) Implicate for a Reactant-State Based Protein-Design Strategy for General Acid/Base Catalysis. *Sci. Rep.* **2018,** *8*, 7042.
(34) Yao, J.; Chen, F.; Guo, H., Qm/Mm Free Energy Simulations of the Reaction Catalysed by (4s)-Limonene Synthase Involving Linalyl Diphosphate (Lpp) Substrate. *Mol. Simul.* **2018,** *44*, 1158-1167.
(35) Yao, J.; Chen, X.; Zheng, F.; Zhan, C.-G., Catalytic Reaction Mechanism for Drug Metabolism in Human Carboxylesterase-1: Cocaine Hydrolysis Pathway. *Mol. Pharm.* **2018,** *15*, 3871-3880.
(36) Wang, X.; Li, Y.; Chen, X.; Zhou, Z.; Yao, J., Human Acetyl-Coa Carboxylase 1 Is an Isomerase: Carboxyl Transfer Is Activated by Catalytic Effect of Isomerization. *J. Phys. Chem. B* **2019,** *123*, 6757-6764.
(37) Wang, X.; Bakanina Kissanga, G. M.; Li, E.; Li, Q.; Yao, J., The Catalytic Mechanism of S-Acyltransferases: Acylation Is Triggered on by a Loose Transition State and Deacylation Is Turned Off by a Tight Transition State. *Phys. Chem. Chem. Phys.* **2019,** *21*, 12163-12172.
(38) Hou, G.; Cui, Q., Stabilization of Different Types of Transition States in a Single Enzyme Active Site: Qm/Mm Analysis of Enzymes in the Alkaline Phosphatase Superfamily. *J. Am. Chem. Soc.* **2013,** *135*, 10457-10469.
(39) Torrie, G. M.; Valleau, J. P., Monte-Carlo Free-Energy Estimates Using Non-Boltzmann Sampling - Application to Subcritical Lennard-Jones Fluid. *Chem. Phys. Lett.* **1974,** *28*, 578-581.
(40) Kumar, S.; Bouzida, D.; Swendsen, R. H.; Kollman, P. A.; Rosenberg, J. M., The Weighted Histogram Analysis Method for Free-Energy Calculations on Biomolecules .1. The Method. *J. Comput. Chem.* **1992,** *13*, 1011-1021.
(41) Zhao, N.; Guan, J.; Forouhar, F.; Tschaplinski, T. J.; Cheng, Z.-M.; Tong, L.; Chen, F., Two Poplar Methyl Salicylate Esterases Display Comparable Biochemical Properties but Divergent

Expression Patterns. *Phytochemistry* **2009,** *70*, 32-39.
(42) Khaliullin, R. Z.; Bell, A. T.; Head-Gordon, M., Analysis of Charge Transfer Effects in Molecular Complexes Based on Absolutely Localized Molecular Orbitals. *J. Chem. Phys.* **2008,** *128*, 184112.
(43) Khaliullin, R. Z.; Bell, A. T.; Head-Gordon, M., Electron Donation in the Water–Water Hydrogen Bond. *Chem. - Eur. J.* **2009,** *15*, 851-855.
(44) Michael B. Smith, J. M., Aliphatic Substitution: Nucleophilic and Organometallic. In *March's Advanced Organic Chemistry*, Sixth ed.; John Wiley & Sons, Inc.: New York, 2006; pp 425-656.
(45) Hou, G.; Cui, Q., Qm/Mm Analysis Suggests That Alkaline Phosphatase (Ap) and Nucleotide Pyrophosphatase/Phosphodiesterase Slightly Tighten the Transition State for Phosphate Diester Hydrolysis Relative to Solution: Implication for Catalytic Promiscuity in the Ap Superfamily. *J. Am. Chem. Soc.* **2011,** *134*, 229-246.
(46) Roston, D.; Demapan, D.; Cui, Q., Leaving Group Ability Observably Affects Transition State Structure in a Single Enzyme Active Site. *J. Am. Chem. Soc.* **2016,** *138*, 7386−7394.
(47) Halder, S.; Satyam, A., Accidental Discovery of a 'Longer-Range' Vinylogous Pummerer-Type Lactonization: Formation of Sulindac Sulfide Lactone from Sulindac. *Tetrahedron Lett.* **2011,** *52*, 1179-1182.
(48) Du, H.; Klessig, D. F., Identification of a Soluble, High-Affinity Salicylic Acid-Binding Protein in Tobacco. *Plant Physiol.* **1997,** *113*, 1319-1327.
(49) Khersonsky, O.; Tawfik, D. S., Enzyme Promiscuity: A Mechanistic and Evolutionary Perspective. *Annu. Rev. Biochem* **2010,** *79*, 471-505.

TOC Graphic